PLANETARY SCIENCE

How Jupiter's unusual magnetospheric topology structures its aurora

Binzheng Zhang[1,2,3]*†, Peter A. Delamere[4†], Zhonghua Yao[5]*, Bertrand Bonfond[6], D. Lin[3], Kareem A. Sorathia[7], Oliver J. Brambles[8], William Lotko[3,9], Jeff S. Garretson[7], Viacheslav G. Merkin[7], Denis Grodent[6], William R. Dunn[10], John G. Lyon[7,11]

Jupiter's bright persistent polar aurora and Earth's dark polar region indicate that the planets' magnetospheric topologies are very different. High-resolution global simulations show that the reconnection rate at the interface between the interplanetary and jovian magnetic fields is too slow to generate a magnetically open, Earth-like polar cap on the time scale of planetary rotation, resulting in only a small crescent-shaped region of magnetic flux interconnected with the interplanetary magnetic field. Most of the jovian polar cap is threaded by helical magnetic flux that closes within the planetary interior, extends into the outer magnetosphere, and piles up near its dawn-side flank where fast differential plasma rotation pulls the field lines sunward. This unusual magnetic topology provides new insights into Jupiter's distinctive auroral morphology.

INTRODUCTION

Impressive auroral displays are seen at every magnetized planet with an atmosphere, but not all aurora are created equal. Earth's aurora is episodic with a usually well-defined oval of bright ultraviolet (UV) luminosity surrounding a dark polar region above 70 to 75° magnetic latitude (MLAT). Jupiter also has an auroral oval encircling the magnetic poles (Fig. 1), but unlike Earth's, it is persistent, and its polar cap—the region poleward of the auroral oval—contains bright, dynamic auroras that account for about half of the emitted UV power (*1*, *2*). Jupiter's polar aurora is often grouped into at least three structures, including a "swirl region" in the center, peppered with dim, intermittent, and chaotic bursts of emissions; an "active region" of flares, bright spots, and arc-like structures on the duskside (*1*, *3*, *4*); and a "dark region" located on the dawnside (*5*, *6*).

Auroras are produced by energetic charged particles that excite emissions when precipitating into the atmosphere. Most of these particles are repelled and trapped in space by the mirror force of the planetary magnetic field, except the few that are forced or scattered into the so-called loss cone and precipitate (*7*). Observed morphological differences in aurora are thus signatures of the different magnetic topologies that define the planetary space environment (the magnetosphere) and the different processes that enable auroral precipitation (*8*). The connection between Earth's aurora and its magnetospheric topology has been explored extensively and is reasonably well understood (*1*, *2*). The jury is still out on the magnetic structure of Jupiter's magnetosphere and what exactly its aurora is telling us about its topology.

The magnetic flux threading Earth's polar cap is typically "open" and interconnected with the interplanetary magnetic field (IMF), a consequence of dayside magnetic reconnection wherein dissipative merging between the IMF and geomagnetic field breaks the frozen-in condition of ideal magnetohydrodynamics (*9*). The polar cap is dark because electrons precipitating into the atmosphere from the extremely low-density plasma populating open field lines have insufficient energy flux to excite intense auroral emissions (*10*). Earth's auroral oval occurs on closed magnetic field lines, meaning the magnetic flux in geospace traces poloidal paths between hemispheres (*11*). The auroral oval is the dominant source of the terrestrial UV auroral emissions, with >70% of the emitted power typically coming from the so-called diffuse aurora and the remainder in the more structured and bright discrete and wave-induced aurora (*12*).

The electron precipitation responsible for Jupiter's auroral oval resembles the discrete and wave-induced aurora at Earth. The causative downward electron flux carries upward-directed magnetic field-aligned currents (FACs), largely generated by the breakdown of plasma corotation on closed magnetic field lines extending (beyond ~20 R_J) (*13*, *14*), a consequence of the fast rotation of the jovian magnetosphere. In analogy with Earth, open field lines are

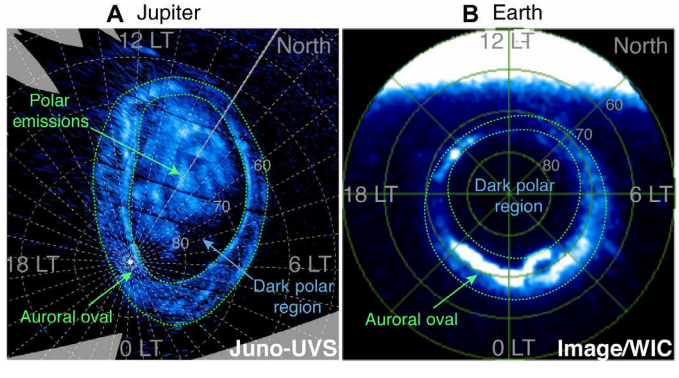

Fig. 1. Polar projections of Northern UV aurora at Jupiter and Earth. (**A**) Juno-UVS, image was acquired on 19 May 2017 at 04:21:56; UVS, ultraviolet spectrograph. (**B**) WIC image was acquired on 14 January 2001 at 05:00:55UT. LT, local time; WIC, wide-field maging camera.

[1]Department of Earth Sciences, The University of Hong Kong, Hong Kong SAR, China. [2]Laboratory for Space Research, The University of Hong Kong, Hong Kong SAR, China. [3]High Altitude Observatory, National Center for Atmospheric Research, Boulder, CO, USA. [4]Geophysical Institute, University of Alaska Fairbanks, Fairbanks, AK, USA. [5]Key Laboratory of Earth and Planetary Physics, Institute of Geology and Geophysics, Chinese Academy of Sciences, Beijing, China. [6]LPAP, Space sciences, Technologies and Astrophysics Research (STAR), Institute Université de Liége (ULiége), Liége, Belgium. [7]Applied Physics Laboratory, Johns Hopkins University, Laural, MD, USA. [8]O.J. Brambles Consulting, Preston, UK. [9]Thayer School of Engineering, Dartmouth College, Hanover, NH, USA. [10]Mullard Space Science Laboratory, University College London, Dorking, UK. [11]Gamera Consulting, Hanover, NH, USA.
*Corresponding author. Email: binzh@hku.hk (B.Z.), zhonghua.yao@uliege.be (Z.Y.)
†These authors contributed equally to this work.

thought to thread most of the region poleward of Jupiter's auroral oval, but this open-flux model is difficult to reconcile with observed precipitation of energetic electrons (*15*) over the polar region, along with ions released by the volcanic moon Io (*16*–*19*).

Thus, Jupiter's bright polar aurora presents quandaries. If it threads open magnetic field lines, why is the precipitating particle energy flux along Jupiter's open field lines so much greater than expected, and how does heavy-ion precipitation access open field lines? A polar cap threaded in part by closed magnetic field lines eliminates these quandaries, but raises questions about the origins of the polar magnetic topology, especially in light of observed reconnection signatures on the dayside and dawnside magnetopause (MP) (magnetospheric interface with the IMF) resembling those at Earth (*20*, *21*). Theoretical studies suggest that the rate of large-scale reconnection at Jupiter may not be fast enough to produce a fully open polar cap (*22*, *23*) with very few polar field lines interconnected with the IMF (*24*, *25*). But it is not clear how or if the polar-region open and closed magnetic field lines are linked and distributed in the magnetosphere.

These questions are not easily addressed with the limited in situ observations available for Jupiter. Physics-based global simulations of the jovian magnetosphere system offer an interpretive framework for the observations (*26*–*30*), particularly the recent in situ measurements from the Juno spacecraft. We investigated the magnetic topology of Jupiter's polar cap using a newly developed global magnetohydrodynamic (MHD) model of the jovian magnetosphere, including its interactions with the interplanetary medium, the effect of mass loading from the volcanic moon Io, and ionosphere-magnetosphere coupling (*31*, *32*). The new results reported here offer a testable model of Jupiter's polar magnetic topology and its magnetic connectivity to the jovian outer magnetosphere and interplanetary medium.

RESULTS

We specified time-stationary, idealized upstream conditions corresponding to a typical "non-compressed" magnetosphere, formed by a Mach 10 solar wind (SW) with a number density of 0.2 cm^{-3}, a speed of 400 km/s, a dynamic pressure of 0.03 nPa, and an east-west IMF component of 0.5 nT. The heavy-ion mass loading from Io is set to 1000 kg/s, which is within the range of empirical estimates (*33*), introduced through the low-altitude boundary of the simulation (6 R_J jovi-centric). The simulation was run for 230 hours (23 jovian days) until the average radial profile of the O+ density is settled into a quasi-steady state, which is inconsistent with the empirical density profile in (*33*) (section A of the Supplementary Materials). The results reported here are derived from the last two planetary spins. We determined the amount of open magnetic flux in the simulated jovian magnetosphere, the connection and linkages of magnetic field lines emanating from the polar and auroral regions, and implications for jovian auroral features.

The reconnection potential $\mathfrak{E}_{\mathbf{reconn}}$ and open magnetic flux Φ are related through Faraday's law

$$\frac{\partial \mathbf{\Phi}}{\partial \mathbf{t}} = -\int_{\mathbf{MP}} \boldsymbol{E} \cdot \boldsymbol{dl} = \mathfrak{E}_{\mathbf{reconn}}$$

$\boldsymbol{E}$ is the electric field along the MP separatrix—the locus of points separating open and closed magnetic field lines (Fig. 2A) (*34*). Integration of the electric potential $\boldsymbol{E} \cdot \boldsymbol{dl}$ projected along the MP separatrix (black curve in Fig. 2B) yields a reconnection potential of $\mathfrak{E}_{\mathbf{reconn}} \approx 508$ kV. This reconnection potential is within the range of estimates based on SW/IMF measurements near Jupiter (*35*).

In quasi-steady state, the transit time (Δt) for SW advection of a newly reconnected and open field line at the dayside MP to the nightside, where it undergoes reconnection again to become a closed field line, is determined from the simulated spatial extent of open flux in the SW (blue lines in Fig. 2) divided by the SW speed: $\Delta t = 279\ R_J/400$ km/s $\approx 48{,}000$ s (13.3 hours). This transit time with the above-calculated $\mathfrak{E}_{reconn}$ in Faraday's law then determines the open flux created by MP reconnection as

$$\Delta \mathbf{\Phi} \approx \Delta \mathbf{t} \cdot \mathfrak{E}_{\mathbf{reconn}} \approx \mathbf{24.4}\ \mathrm{GWb}$$

This open flux is approximately 9% of the total dipole magnetic flux [259 Giga Weber (GWb)] threading the simulated jovian polar cap (PC), taken to be the area in Fig. 3A above ≈82° MLAT. Flux-equivalence mappings of the low-altitude footpoints of magnetic fields measured in the jovian magnetosphere (*36*) suggest an 11° symmetric-circle equivalent of the observationally ill-defined, asymmetric PC. The mapped equivalent flux within the PC, assumed to be fully open in (*36*), is estimated at 700 to 730 GWb and is about 50% larger than the dipole equivalent flux of 488 GWb for a PC within 11° of the pole. The generation of such large open flux, given the simulation value for $\mathfrak{E}_{\mathbf{reconn}}$, requires an MP merging distance of order 4 astronomical unit (AU), wherein the field lines most likely become Alfvénically disconnected from Jupiter. Therefore, the spatial distribution of Jupiter's open PC flux must be very different from that of Earth's PC. Note that due to the use of an azimuthally symmetric, point dipole field as the intrinsic jovian magnetic field in the simulation, the low-altitude mapping of the FACs in the simulated jovian magnetosphere does not exhibit local time (LT) asymmetry as the observed auroral emission, especially in the Northern Hemisphere. The use of a non-dipolar magnetic field will influence the amount and spatial distribution of the open flux including hemispheric asymmetrics, but it is unlikely a dominant effect since the open magnetic flux is mostly generated by the merging of the upstream IMF with the dipole component of the jovian magnetic field.

Figure 3A shows the spatial distribution of open flux and FACs derived from the magnetic field averaged over two jovian days and traced to the low-altitude boundary of the simulation. Instead of forming a single circular-shaped open PC as at Earth, the simulated average open flux at Jupiter threads two disjoint polar regions: (i) a crescent-shaped region spanning ≈82 to 83° MLAT and extending from dusk to noon in LT between regions of upward and downward FAC and (ii) a duskside patch region above 85° MLAT. The crescent-shaped open flux is magnetically connected to the dawnside IMF (Fig. 2A) with an average magnetic flux of 23.4 GWb in excellent agreement with the above estimate from Faraday's law. The average spatial distribution of the crescent-shaped open flux is similar to the measured crescent-shaped polar region devoid of auroral emissions (*37*, *38*). A similar narrow region in the measured ion wind with little velocity in the inertial frame is also seen in Saturn's magnetosphere, which is likely under SW control (*39*). The simulated crescent exhibits less MLAT distortion than the void in Hubble Space Telescope images, probably due to the use of an axisymmetric dipole magnetic field; however, the simulated and observed crescents are both more or less fixed in LT, in contrast with other polar features (*40*). The high-latitude patch region above 85° MLAT contains about 19% (5.5 GWb) of the total open flux. If the simulated PC in

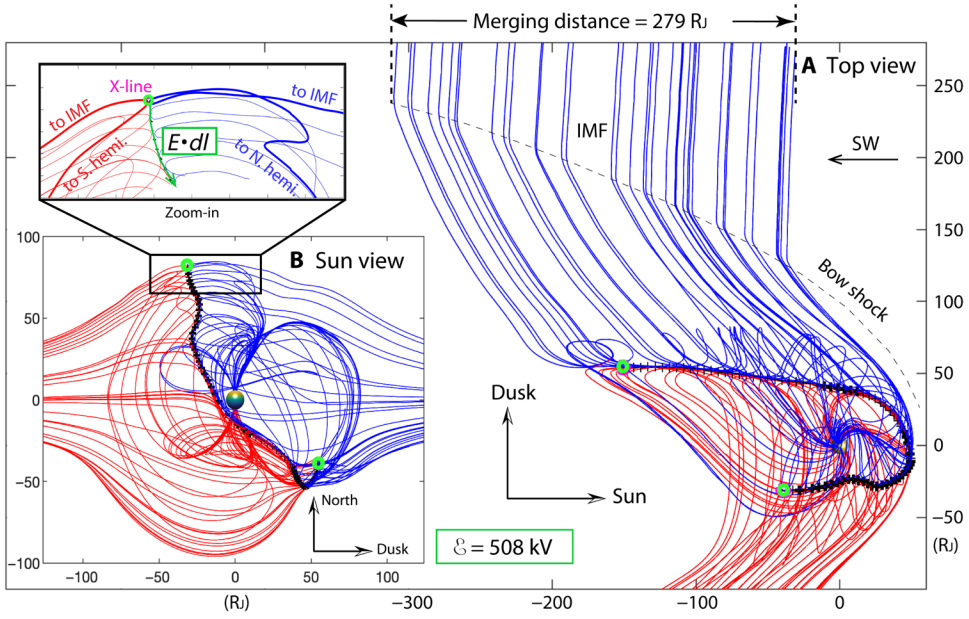

Fig. 2. Jovian magnetic field lines connected to the IMF after undergoing reconnection at the MP. Black curves (magnetic separatrix) separate topological classes: open, closed, and IMF. View from: Northern Hemisphere down onto the pole (**A**) and Sun (**B**), with zoom-in example of a reconnection site. Blue/red field lines emerge from the Northern/Southern Hemisphere. The green circles locate the termination of the MP reconnection separatrix.

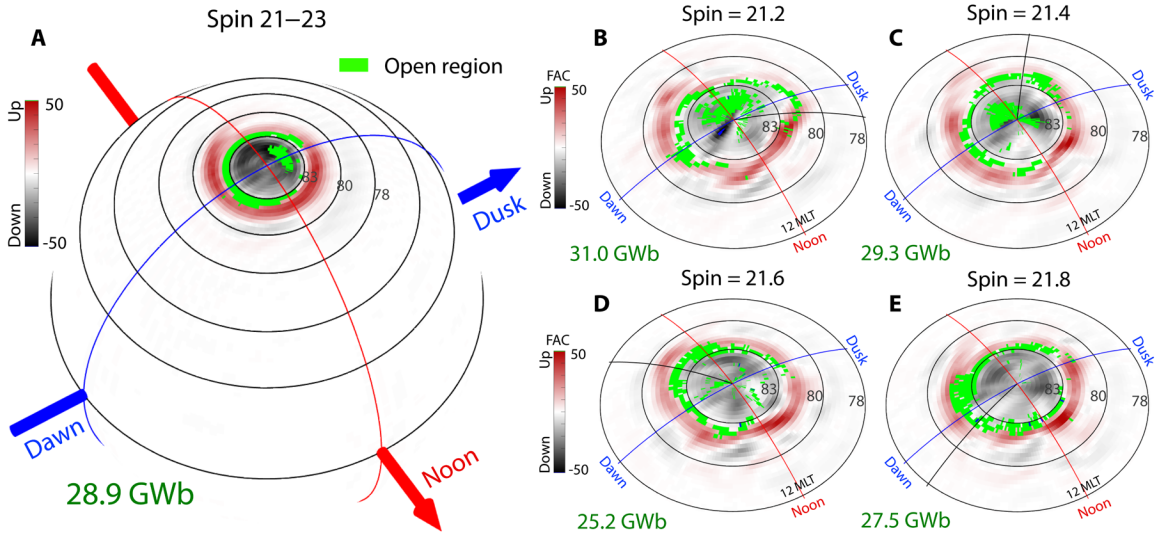

Fig. 3. Distributions of PC open flux and FAC density. (**A**) Distributions averaged over simulation days 21 to 23. Instantaneous distributions at diurnal time 21.2 (**B**), 21.4 (**C**), 21.6 (**D**), and 21.8 (**E**). The open flux region is shown in green. Upward (downward) FACs are shown in red (gray). Projections are on the 6 R_J spherical surface versus MLAT and magnetic local time (MLT) with total open flux (in GWb) given at the lower left.

Fig. 3A is taken to be the area above 82° MLAT, then 89% of the PC flux is closed in the simulation.

Both the crescent and patch regions of the jovian open flux exhibit dynamic variations. Figure 3 (B to E) shows snapshots of the distributions of open flux together with FACs derived at different phases of planetary spin 21. The open flux of the instantaneous crescent region near 82° to 83° MLAT varies from 18.6 to 25.2 GWb. The patch region is more intermittent with a highly variable spatial distribution; e.g., its open flux is 3.7 to 11.0 GWb during the first half of spin 21 and almost disappears during the second half of spin 21 (0.3 to 3.7 GWb). What exactly controls the patch region deserves further investigation. It is likely generated via complicated interactions between magnetotail reconnection and ionospheric electrodynamics, regulated by the strength of the dipole, angular speed of planetary rotation, orientation of the upstream IMF, and spatial gradients in ionospheric conductivity (*41*).

Figure 4 shows the two-day average topology of simulated jovian magnetic field lines traced from four different sets of footpoints at the northern low-altitude simulation boundary. The green open field lines have footpoints in the crescent region and are connected

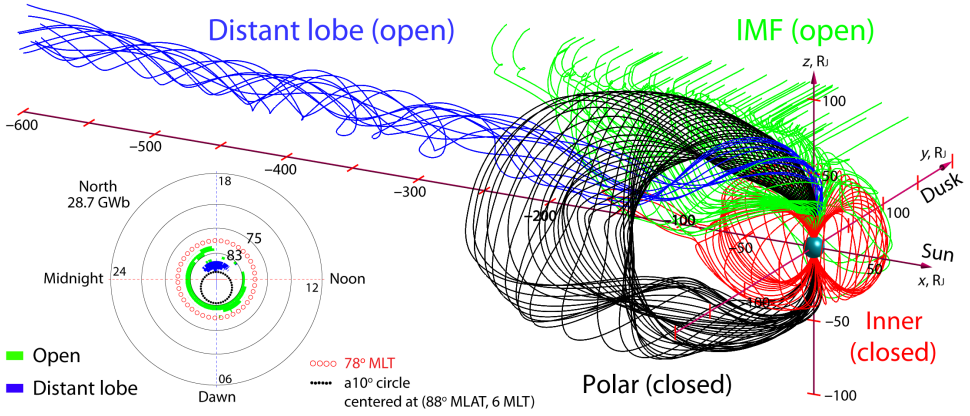

Fig. 4. Different topological classes of jovian magnetic field lines averaged over simulation days 21 to 23. Illustrative field lines emerge from four low-altitude sets in the Northern Hemisphere (lower left). Red: 78° MLAT. Green: crescent region. Blue: patch region. Black: closed polar cap.

to the IMF. They are created by MP reconnection and are mostly under SW control, which may be related to the "zero inertial velocity" region in line-of-sight ion wind measurements in the jovian polar ionosphere (*40*, *42*). The blue field lines originate from the duskside patch region and map to the distant tail beyond 600 R_J. The downward FACs flowing along these helical open field lines (winding counterclockwise when looking upward) are generated by differential rotation of the polar ionosphere due to the frozen-in condition of the flux tubes in ideal MHD (*43*, *44*). Their long extent is consistent with observations of Jupiter's very elongated magnetotail (*45*). This transient region could be possibly related to the "old core" open field lines predicted based on observations of the UV emission (*38*, *46*). The red closed field lines have footpoints at 80° MLAT. They map outward to 35 to 40 R_J in the middle magnetosphere and return to the southern boundary (ionosphere). The black field lines emerging from Jupiter's polar region illustrate one of the more unusual features of jovian magnetic topology. These helical, closed field lines connect the two polar regions through the dawnside outer magnetosphere and have no counterpart in the terrestrial magnetosphere. This topological feature occurs because the time scale for reconnection to retain open flux, estimated above as 48,100 s, is too slow to generate a complete open PC in a single jovian rotation of a period of 36,540 s. Thus, the black polar field lines in Fig. 4 cannot access the IMF at the MP and remain closed. These magnetic flux pile-up on the dawnside flank are bent sunward by Jupiter's differentially rotating plasma and develop a low-latitude boundary layer through viscous stresses at the MP boundary (*25*).

DISCUSSION

Complex dawnside magnetic structures have also been found in other global simulations of the jovian magnetosphere (*47*, *48*). Their geodesic curvature is produced by field-perpendicular currents that flow toward the planet, balance the inertia of differential plasma rotation via a tailward MHD Lorentz force, and are diverted into downward PC FACs (Fig. 3), in a manner similar to what occurs in Earth's low-latitude boundary layer (*49*). This giant volume of trapped jovian magnetospheric plasma connects the dynamics of the two polar hemispheres. In the geospace, these variabilities stimulate Alfvénic perturbations, field line resonant oscillations, and associated particle acceleration to power aurora (*50*). In the jovian magnetosphere, the observed 2- to 3-min oscillations of jovian polar auroral emissions (*3*) arise naturally on these closed field lines, which should also support hemispherically conjugate aurora. Note that the magnetic topology shown in Fig. 4 exhibits the average direction of the magnetic field vector corresponding to steady state, east-west IMF conditions. Numerical experiments have shown that the closed polar cap flux tube is a robust feature under a variety of IMF orientations driven by nominal SW conditions at Jupiter, as well as ionospheric conductance and mass loading rate from the Io plasma.

Jupiter's unusual magnetospheric topology requires care when interpreting the sources of the planet's polar aurora. For example, some or all of the dayside "active region" (*51*) maps along closed polar field lines (Fig. 4) into the dawn-to-midnight equatorial magnetosphere. Auroral activity in this region might then be attributable to flankside boundary layer and/or nightside magnetotail dynamics rather than dayside reconnection, as is typical at Earth.

MATERIALS AND METHODS

We use the Grid Agnostic MHD for Extended Research Applications (GAMERA) global model (*32*) to simulate the interaction of the SW and IMF with the jovian space environment—the volume of space where the jovian magnetic field dominates the IMF. The model is based on equations of multi-fluid MHD (*52*, *53*), including (i) a dipole magnetic field embedded at the center of Jupiter to represent the planet's intrinsic magnetic field; (ii) supersonic upwind conditions representing the SW and embedded IMF powering the interaction; (iii) low-altitude boundary conditions representing the closure of magnetospheric FACs in the jovian ionosphere; (iv) rotation of the planet at the low-altitude boundary imposed through an electrostatic potential; (v) a plasma source representing heavy-ion mass loading from the Io plasma torus; and (vi) numerical resistivity that enables magnetic reconnection in ideal MHD.

The computational volume of the simulation is a stretched sphere of length 1200 R_J along the *x* axis of the solar magnetic (SM) coordinate system of Jupiter and 400 R_J in the directions perpendicular to the *x* axis. A spherical volume of radius 6 R_J is cut out inside the distorted spherical computational domain. The sphere is centered on Jupiter, 100 R_J downstream from the upwind surface where the SW/IMF conditions are imposed. The three-dimensional view of the computational grid is shown in section A of the Supplementary Materials (fig. S1).

The primary computational technique is explicit, finite volume MHD. The code uses Adams-Bashforth time marching with an upwind, seventh-order spatial reconstruction. In addition, nonlinear numerical switches based on the Partial Donor Method are used to maintain the total variation diminishing (TVD) property. The constrained transport technique is used to achieve zero numerical divergence of the magnetic field while fulfilling this TVD condition for the system of equations (*54*). The finite volume technique allows the code to complete its calculation on a non-orthogonal numerical grid with cells adapted to the configuration of the jovian magnetosphere, e.g., cells that are smaller in the inner magnetosphere and across the nominal MP than parallel to it. The computational grid used for the runs in this paper has 256 × 256 × 256 cells. The grid is spherical polar near the low-altitude boundary with axis of symmetry along the SM x axis and with indices ($i \times j \times k$) corresponding approximately to the spherical ($r \times \theta \times \phi$) coordinates (radial × meridional × azimuthal) with horizontal resolution mapped to the ionosphere of approximately 0.3° × 0.15° in MLT and MLAT.

A numerical resistivity enables magnetic reconnection in the code when and where magnetic gradients reach the grid scale, which is approximately 0.16 R_J near the x-line on the dayside MP for the 256 × 256 × 256 resolution computational grid. The resulting reconnection electric field is typically of order $0.1 v_A B_{in}$, in terms of the Alfvén speed v_A and magnetic field B_{in} in the reconnection inflow region. This practically universal scaling indicates that the reconnection rate is not caused by changes in numerical dissipation and that the numerical resistivity is simulating large-scale aspects of reconnection appropriately (*34*). It has also been shown that the global rate of dayside reconnection in the magnetosphere is controlled by upstream conditions in the global simulation model rather than the grid resolution of the simulation (*55*).

It is well known that one of the issues in simulating space plasmas is that dimensionless quantities, like the Lundquist number, are extremely large, since the behavior of the simulated system will drastically change going from a low Lundquist number to a high Lundquist number. It is impossible to add a meaningful physical resistivity to calculating a system like Jupiter that does not create a simulation very far from the true system's behavior. For global models, one standard way around this is to depend on numerical effects at the grid scale either positing a very large resistivity in a localized area or by using averaging error of oppositely directed fields. In either case, it is possible to create simulations with a mesoscale and turbulent structure that a constant resistivity would not show. It is also worth noting that the local reconnection rate in these models is the same as fine-scaled Hall or PIC results, which is approximately $0.1 * v_{in} * B$ of the inflow region, as shown by many previous studies (*34*, *55*, *56*), suggesting that the code is simulating the large-scale configuration of the reconnection process, in terms of the rate of reconnection, reasonably well through the conservation of mass, momentum, and magnetic flux.

SUPPLEMENTARY MATERIALS

Supplementary material for this article is available at http://advances.sciencemag.org/cgi/content/full/7/15/eabd1204/DC1

REFERENCES AND NOTES

1. D. Grodent, J. T. Clarke, J. H. Waite Jr., S. W. H. Cowley, J.-C. Gérard, J. Kim, Jupiter's polar auroral emissions. *J. Geophys. Res. Space Physics* **108**, 1366 (2003).
2. J. D. Nichols, J. T. Clarke, J. C. Gérard, D. Grodent, K. C. Hansen, Variation of different components of Jupiter's auroral emission. *J. Geophys. Res. Space Physics* **114**, A06210 (2009).
3. B. Bonfond, M. F. Vogt, J.-C. Gérard, D. Grodent, A. Radioti, V. Coumans, Quasi-periodic polar flares at Jupiter: A signature of pulsed dayside reconnections? *Geophys. Res. Lett.* **38**, L02104 (2011).
4. D. Grodent, J. T. Clarke, J. Kim, J. H. Waite Jr., S. W. H. Cowley, Jupiter's main auroral oval observed with HST-STIS. *J. Geophys. Res. Space Physics* **108**, 1389 (2003).
5. T. S. Stallard, S. Miller, S. W. H. Cowley, E. J. Bunce, Jupiter's polar ionospheric flows: Measured intensity and velocity variations poleward of the main auroral oval. *Geophys. Res. Lett.* **30**, 1221 (2003).
6. T. Stallard, S. Miller, G. Millward, R. D. Joseph, On the dynamics of the jovian ionosphere and thermosphere: I. The measurement of ion winds. *Icarus* **154**, 475–491 (2001).
7. L. R. Lyons, Magnetospheric processes leading to precipitation. *Space Sci. Rev.* **80**, 109–132 (1997).
8. G. Paschmann, S. Haaland, R. Treumann, *Auroral Plasma Physics* (Springer Science & Business Media, 2012), vol. 15.
9. J. W. Dungey, Interplanetary magnetic field and the auroral zones. *Phys. Rev. Lett.* **6**, 47–48 (1961).
10. L. C. Evans, E. C. Stone, Electron polar cap and the boundary of open geomagnetic field lines. *J. Geophys. Res.* **77**, 5580–5584 (1972).
11. Y. I. Feldstein, G. V. Starkov, The auroral oval and the boundary of closed field lines of geomagnetic field. *Planet. Space Sci.* **18**, 501–508 (1970).
12. P. T. Newell, T. Sotirelis, S. Wing, Diffuse, monoenergetic, and broadband aurora: The global precipitation budget. *J. Geophys. Res. Space Physics* **114**, A09207 (2009).
13. T. W. Hill, The Jovian auroral oval. *J. Geophys. Res. Space Physics* **106**, 8101–8107 (2001).
14. S. W. H. Cowley, E. J. Bunce, Origin of the main auroral oval in Jupiter's coupled magnetosphere–ionosphere system. *Planet. Space Sci.* **49**, 1067–1088 (2001).
15. B. H. Mauk, D. K. Haggerty, C. Paranicas, G. Clark, P. Kollmann, A. M. Rymer, D. G. Mitchell, S. J. Bolton, S. M. Levin, A. Adriani, F. Allegrini, F. Bagenal, J. E. P. Connerney, G. R. Gladstone, W. S. Kurth, D. J. McComas, D. Ranquist, J. R. Szalay, P. Valek, Juno observations of energetic charged particles over Jupiter's polar regions: Analysis of monodirectional and bidirectional electron beams. *Geophys. Res. Lett.* **44**, 4410–4418 (2017).
16. G. Branduardi-Raymont, A. Bhardwaj, R. F. Elsner, G. R. Gladstone, G. Ramsay, P. Rodriguez, R. Soria, J. H. Waite Jr., T. E. Cravens, A study of Jupiter's aurorae with XMM-Newton. *Astron. Astrophys.* **463**, 761–774 (2007).
17. G. Clark, B. H. Mauk, D. Haggerty, C. Paranicas, P. Kollmann, A. Rymer, E. J. Bunce, S. W. H. Cowley, D. G. Mitchell, G. Provan, R. W. Ebert, F. Allegrini, F. Bagenal, S. Bolton, J. Connerney, S. Kotsiaros, W. S. Kurth, S. Levin, D. J. McComas, J. Saur, P. Valek, Energetic particle signatures of magnetic field-aligned potentials over Jupiter's polar regions. *Geophys. Res. Lett.* **44**, 8703–8711 (2017).
18. R. F. Elsner, N. Lugaz, J. H. Waite Jr., T. E. Cravens, G. R. Gladstone, P. Ford, D. Grodent, A. Bhardwaj, R. J. MacDowall, M. D. Desch, T. Majeed, Simultaneous Chandra X ray, Hubble Space Telescope ultraviolet, and Ulysses radio observations of Jupiter's aurora. *J. Geophys. Res. Space Physics* **110**, A01207 (2005).
19. D. K. Haggerty, B. H. Mauk, C. P. Paranicas, G. Clark, P. Kollmann, A. M. Rymer, S. J. Bolton, J. E. P. Connerney, S. M. Levin, Juno/JEDI observations of 0.01 to >10 MeV energetic ions in the Jovian auroral regions: Anticipating a source for polar X-ray emission. *Geophys. Res. Lett.* **44**, 6476–6482 (2017).
20. D. J. Gershman, G. A. DiBraccio, J. E. P. Connerney, G. Hospodarsky, W. S. Kurth, R. W. Ebert, J. R. Szalay, R. J. Wilson, F. Allegrini, P. Valek, D. J. McComas, F. Bagenal, S. Levin, S. J. Bolton, Juno observations of large-scale compressions of Jupiter's dawnside magnetopause. *Geophys. Res. Lett.* **44**, 7559–7568 (2017).
21. R. W. Ebert, F. Allegrini, F. Bagenal, S. J. Bolton, J. E. P. Connerney, G. Clark, G. A. DiBraccio, D. J. Gershman, W. S. Kurth, S. Levin, P. Louarn, B. H. Mauk, D. J. McComas, M. Reno, J. R. Szalay, M. F. Thomsen, P. Valek, S. Weidner, R. J. Wilson, Accelerated flows at Jupiter's magnetopause: Evidence for magnetic reconnection along the dawn flank. *Geophys. Res. Lett.* **44**, 4401–4409 (2017).
22. M. Desroche, F. Bagenal, P. A. Delamere, N. Erkaev, Conditions at the expanded Jovian magnetopause and implications for the solar wind interaction. *J. Geophys. Res. Space Physics* **117**, A07202 (2012).
23. A. Masters, Model-based assessments of magnetic reconnection and Kelvin-Helmholtz instability at Jupiter's magnetopause. *J. Geophys. Res. Space Physics* **122**, 11,154–11,174 (2017).
24. P. A. Delamere, F. Bagenal, Solar wind interaction with Jupiter's magnetosphere. *J. Geophys. Res. Space Physics* **115**, A10201 (2010).
25. P. A. Delamere, F. Bagenal, Magnetotail structure of the giant magnetospheres: Implications of the viscous interaction with the solar wind. *J. Geophys. Res. Space Physics* **118**, 7045–7053 (2013).
26. E. Chané, J. Saur, S. Poedts, Modeling Jupiter's magnetosphere: Influence of the internal sources. *J. Geophys. Res. Space Physics* **118**, 2157–2172 (2013).
27. T. Ogino, R. J. Walker, M. G. Kivelson, A global magnetohydrodynamic simulation of the Jovian magnetosphere. *J. Geophys. Res. Space Physics* **103**, 225–235 (1998).
28. Y. Sarkango, X. Jia, G. Toth, Global MHD simulations of the response of Jupiter's magnetosphere and ionosphere to changes in the solar wind and IMF. *J. Geophys. Res. Space Physics* **124**, 5317–5341 (2019).

29. R. J. Walker, T. Ogino, M. G. Kivelson, Magnetohydrodynamic simulations of the effects of the solar wind on the Jovian magnetosphere. *Planet. Space Sci.* **49**, 237–245 (2001).
30. Y. Wang, X. Guo, B. Tang, W. Li, C. Wang, Modeling the Jovian magnetosphere under an antiparallel interplanetary magnetic field from a global MHD simulation. *Earth Planet. Phys.* **2**, 303–309 (2018).
31. B. Zhang, P. A. Delamere, X. Ma, B. Burkholder, M. Wiltberger, J. G. Lyon, V. G. Merkin, K. A. Sorathia, Asymmetric Kelvin-Helmholtz instability at Jupiter's magnetopause boundary: Implications for corotation-dominated systems. *Geophys. Res. Lett.* **45**, 56–63 (2018).
32. B. Z. Zhang, K. A. Sorathia, J. G. Lyon, V. G. Merkin, J. S. Garretson, M. Wiltberger, GAMERA: A three-dimensional finite-volume MHD solver for non-orthogonal curvilinear geometries. *Astrophys. J. Suppl. Ser.* **244**, 20 (2019).
33. F. Bagenal, P. A. Delamere, Flow of mass and energy in the magnetospheres of Jupiter and Saturn. *J. Geophys. Res. Space Physics* **116**, A05209 (2011).
34. J. E. Ouellette, B. N. Rogers, M. Wiltberger, J. G. Lyon, Magnetic reconnection at the dayside magnetopause in global Lyon-Fedder-Mobarry simulations. *J. Geophys. Res. Space Physics* **115**, A08222 (2010).
35. J. D. Nichols, S. W. H. Cowley, D. J. McComas, Magnetopause reconnection rate estimates for Jupiter's magnetosphere based on interplanetary measurements at ~5AU. *Ann. Geophys.* **24**, 393–406 (2006).
36. M. F. Vogt, M. G. Kivelson, K. K. Khurana, R. J. Walker, B. Bonfond, D. Grodent, A. Radioti, Improved mapping of Jupiter's auroral features to magnetospheric sources. *J. Geophys. Res. Space Physics* **116**, A03220 (2011).
37. B. G. Swithenbank-Harris, J. D. Nichols, E. J. Bunce, Jupiter's dark polar region as observed by the Hubble space telescope during the Juno approach phase. *J. Geophys. Res. Space Physics* **124**, 9094–9105 (2019).
38. T. S. Stallard, J. T. Clarke, H. Melin, S. Miller, J. D. Nichols, J. O'Donoghue, R. E. Johnson, J. E. P. Connerney, T. Satoh, M. Perry, Stability within Jupiter's polar auroral 'Swirl region' over moderate timescales. *Icarus* **268**, 145–155 (2016).
39. T. S. Stallard, S. Miller, L. M. Trafton, T. R. Geballe, R. D. Joseph, Ion winds in Saturn's southern auroral/polar region. *Icarus* **167**, 204–211 (2004).
40. R. E. Johnson, T. S. Stallard, H. Melin, J. D. Nichols, S. W. H. Cowley, Jupiter's polar ionospheric flows: High resolution mapping of spectral intensity and line-of-sight velocity of H_3^+ ions. *J. Geophys. Res. Space Physics* **122**, 7599–7618 (2017).
41. W. Lotko, R. H. Smith, B. Z. Zhang, J. E. Ouellette, O. J. Brambles, J. G. Lyon, Ionospheric control of magnetotail reconnection. *Science* **345**, 184–187 (2014).
42. R. E. Johnson, H. Melin, T. S. Stallard, C. Tao, J. D. Nichols, M. N. Chowdhury, Mapping H_3^+ temperatures in Jupiter's Northern auroral ionosphere using VLT-CRIRES. *J. Geophys. Res. Space Physics* **123**, 5990–6008 (2018).
43. S. E. Milan, E. J. Bunce, S. W. H. Cowley, C. M. Jackman, Implications of rapid planetary rotation for the Dungey magnetotail of Saturn. *J. Geophys. Res. Space Physics* **110**, A03209 (2005).
44. J. Isbell, A. J. Dessler, J. H. Waite Jr., Magnetospheric energization by interaction between planetary spin and the solar wind. *J. Geophys. Res. Space Physics* **89**, 10716–10722 (1984).
45. W. S. Kurth, J. D. Sullivan, D. A. Gurnett, F. L. Scarf, H. S. Bridge, E. C. Sittler Jr., Observations of Jupiter's distant magnetotail and wake. *J. Geophys. Res. Space Physics* **87**, 10373–10383 (1982).
46. T. S. Stallard, K. H. Baines, H. Melin, T. J. Bradley, L. Moore, J. O'Donoghue, S. Miller, M. N. Chowdhury, S. V. Badman, H. J. Allison, E. Roussos, Local-time averaged maps of H_3^+ emission, temperature and ion winds. *Philos. Trans. Royal Soc. A* **377**, 20180405 (2019).
47. T. Miyoshi, K. Kusano, A global MHD simulation of the Jovian magnetosphere interacting with/without the interplanetary magnetic field. *J. Geophys. Res. Space Physics* **106**, 10723–10742 (2001).
48. T. Moriguchi, A. Nakamizo, T. Tanaka, T. Obara, H. Shimazu, Current systems in the Jovian magnetosphere. *J. Geophys. Res. Space Physics* **113**, (2008).
49. B. U. Ö. Sonnerup, Theory of the low-latitude boundary layer. *J. Geophys. Res. Space Physics* **85**, 2017–2026 (1980).
50. A. Keiling, J. R. Wygant, C. A. Cattell, F. S. Mozer, C. T. Russell, The global morphology of wave poynting flux: Powering the aurora. *Science* **299**, 383–386 (2003).
51. D. Grodent, A brief review of ultraviolet auroral emissions on giant planets. *Space Sci. Rev.* **187**, 23–50 (2015).
52. O. J. Brambles, W. Lotko, B. Zhang, M. Wiltberger, J. Lyon, R. J. Strangeway, Magnetosphere sawtooth oscillations induced by ionospheric outflow. *Science* **332**, 1183–1186 (2011).
53. M. Wiltberger, W. Lotko, J. G. Lyon, P. Damiano, V. Merkin, Influence of cusp O^+ outflow on magnetotail dynamics in a multifluid MHD model of the magnetosphere. *J. Geophys. Res. Space Phys.* **115**, A00J05 (2010).
54. J. G. Lyon, J. A. Fedder, C. M. Mobarry, The Lyon-Fedder-Mobarry (LFM) global MHD magnetospheric simulation code. *J. Atmos. Sol. Terr. Phys.* **66**, 1333–1350 (2004).
55. B. Zhang, O. J. Brambles, P. A. Cassak, J. E. Ouellette, M. Wiltberger, W. Lotko, J. G. Lyon, Transition from global to local control of dayside reconnection from ionospheric-sourced mass loading. *J. Geophys. Res. Space Phys.* **122**, 9474–9488 (2017).
56. J. E. Ouellette, O. J. Brambles, J. G. Lyon, W. Lotko, B. N. Rogers, Properties of outflow-driven sawtooth substorms. *J. Geophys. Res. Space Physics* **118**, 3223–3232 (2013).
57. R. H. Varney, M. Wiltberger, B. Zhang, W. Lotko, J. Lyon, Influence of ion outflow in coupled geospace simulations: 1. Physics-based ion outflow model development and sensitivity study. *J. Geophys. Res. Space Phys.* **121**, 9671–9687 (2016).
58. V. G. Merkin, J. G. Lyon, Effects of the low-latitude ionospheric boundary condition on the global magnetosphere. *J. Geophys. Res. Space Phys.* **115**, A10202 (2010).
59. L. C. Ray, R. E. Ergun, P. A. Delamere, F. Bagenal, Magnetosphere-ionosphere coupling at Jupiter: A parameter space study. *J. Geophys. Res. Space Physics* **117**, A01205 (2012).
60. S. V. Badman, S. W. H. Cowley, Significance of Dungey-cycle flows in Jupiter's and Saturn's magnetospheres, and their identification on closed equatorial field lines. *Ann. Geophys.* **25**, 941–951 (2007).
61. C. M. Komar, P. A. Cassak, J. C. Dorelli, A. Glocer, M. M. Kuznetsova, Tracing magnetic separators and their dependence on IMF clock angle in global magnetospheric simulations. *J. Geophys. Res. Space Physics* **118**, 4998–5007 (2013).
62. R. E. Lopez, R. Bruntz, E. J. Mitchell, M. Wiltberger, J. G. Lyon, V. G. Merkin, Role of magnetosheath force balance in regulating the dayside reconnection potential. *J. Geophys. Res. Space Phys.* **115**, A12216 (2010).
63. O. J. Brambles, W. Lotko, P. A. Damiano, B. Zhang, M. Wiltberger, J. Lyon, Effects of causally driven cusp O^+ outflow on the storm time magnetosphere-ionosphere system using a multifluid global simulation. *J. Geophys. Res. Space Phys.* **115**, A00J04 (2010).
64. R. E. Lopez, The integrated dayside merging rate is controlled primarily by the solar wind. *J. Geophys. Res. Space Physics* **121**, 4435–4445 (2016).

Acknowledgments

Funding: B.Z. was supported by the RGC Early Career Scheme (27302018) and the General Research Fund (17300719 and 17308520) and the Excellent Young Scientists Fund (Hong Kong and Macau) of the National Natural Science Foundation of China (41922060). P.D. was supported by NASA grants (80NSSC20K1279 and 80NSSC19K0822). Z.Y. was supported by the Key Research Program of the Institute of Geology and Geophysics, CAS (201904). NCAR is a major facility sponsored by the US National Science Foundation under Cooperative Agreement no. 1852977 and sponsored D.L. as a postdoctoral fellow through its Advanced Study Program and computing resources through its Computational and Information Systems Laboratory (UJHB0015). D.G. was supported by the PRODEX program managed by ESA in collaboration with the Belgian Federal Science Policy Office. We are grateful to NASA and contributing institutions which have made the Juno mission possible. This work was funded by NASA's New Frontiers Program for Juno via contract with the Southwest Research Institute. We thank the International Space Science Institute in Beijing (ISSI-BJ) for supporting and hosting the meetings of the International Team on "The morphology of auroras at Earth and giant planets: characteristics and their magnetospheric implications," during which the discussions leading/contributing to this publication were initiated/held. Funding was provided by RGC Early Career Scheme (27302018), the General Research Fund (17300719 and 17308520), and the Excellent Young Scientists Fund (Hong Kong and Macau) of NSFC (41922060) and NASA (80NSSC20K1279 and 80NSSC19K0822). **Author contributions:** B.Z. wrote the paper, P.A.D., Z.Y., O.J.B., and W.L. contributed to the analysis and writing; D.L., K.A.S., V.G.M., J.S.G., and J.G.L. developed the global simulation code; B.B., D.G., and W.R.D. provided the Juno and HST data and analysis. **Competing interests:** The authors declare that they have no competing interests. **Data and materials availability:** All data needed to evaluate the conclusions in the paper are present in the paper and/or the Supplementary Materials. The Juno UVS data used in this paper are archived in NASA's Planetary Data System Atmospheres Node: https://pds-atmospheres.nmsu.edu/PDS/data/jnouvs_3001. The WIC, SI12, and SI13 images can be accessed online (at https://spdf.gsfc.nasa.gov/pub/data/image/fuv/) and were processed using the FUVIEW3 software (http://sprg.ssl.berkeley.edu/image/). Simulation codes and data are available from B.Z. upon request.

Submitted 2 June 2020
Accepted 22 February 2021
Published 9 April 2021
10.1126/sciadv.abd1204

Citation: B. Zhang, P. A. Delamere, Z. Yao, B. Bonfond, D. Lin, K. A. Sorathia, O. J. Brambles, W. Lotko, J. S. Garretson, V. G. Merkin, D. Grodent, W. R. Dunn, J. G. Lyon, How Jupiter's unusual magnetospheric topology structures its aurora. *Sci. Adv.* **7**, eabd1204 (2021).